

Single-ion anisotropy in the gadolinium pyrochlores studied by an electron paramagnetic resonance

V. N. Glazkov,^{1,2} M. E. Zhitomirsky,¹ A. I. Smirnov,²
H.-A. Krug von Nidda,³ A. Loidl,³ C. Marin,¹ and J.-P. Sanchez¹

¹*Commissariat à l'Energie Atomique, DSM/DRFMC/SPSMS, 38054 Grenoble, Cedex 9, France*

²*P. L. Kapitza Institute for Physical Problems RAS, 117334 Moscow, Russia*

³*Experimentalphysik V, EKM, Institut für Physik,
Universität Augsburg, 86135 Augsburg, Germany*

(Dated: October 2, 2018)

The electron paramagnetic resonance is used to measure the single-ion anisotropy of Gd^{3+} ions in the pyrochlore structure of $(\text{Y}_{1-x}\text{Gd}_x)_2\text{Ti}_2\text{O}_7$. A rather strong easy-plane type anisotropy is found. The anisotropy constant D is comparable to the exchange integral J in the prototype $\text{Gd}_2\text{Ti}_2\text{O}_7$, $D \simeq 0.75J$, and exceeds the dipolar energy scale. Physical implications of an easy-plane anisotropy for a pyrochlore antiferromagnet are considered. We calculate the magnetization curves at $T = 0$ and discuss phase transitions in magnetic field.

PACS numbers: 76.30.Kg, 75.50.Ee, 75.10.Hk

Pyrochlore antiferromagnets have been actively studied in the past due to their unusual properties.¹ The magnetic ions in these compounds form a network of corner-sharing tetrahedra, which is prone to a high degree of geometric frustration. The ground state of a classical Heisenberg antiferromagnet on a pyrochlore lattice is macroscopically degenerate and remains disordered.² Since weaker residual interactions are always present in real magnetic materials, an important question is about a separation of energy scales. The corresponding knowledge helps to clarify how the macroscopic entropy freezes as $T \rightarrow 0$ and what type of magnetically ordered, spin-liquid, or glassy state is eventually stabilized.

Gadolinium pyrochlores $\text{Gd}_2\text{Ti}_2\text{O}_7$ and $\text{Gd}_2\text{Sn}_2\text{O}_7$ are considered to be the best realizations of the Heisenberg model on a pyrochlore lattice, since Gd^{3+} is, nominally, in a $^8S_{7/2}$ state with completely frozen orbital degrees of freedom. Both compounds order at temperatures of about 1 K,^{3,4,5} while $\text{Gd}_2\text{Ti}_2\text{O}_7$ exhibits also multiple phases in magnetic field.^{4,6} This has been attributed to weaker dipolar interactions between the $S = 7/2$ gadolinium spins,^{3,7,8} though no unambiguous explanation neither of the phase diagram of $\text{Gd}_2\text{Ti}_2\text{O}_7$ nor of the neutron-diffraction measurements⁹ has been presented.

Single-ion effects have so far been neglected for the two gadolinium pyrochlores. However, strong spin-orbit coupling of the $4f$ electrons breaks the LS -scheme of the energy levels of the Gd^{3+} ion and mixes the $^8S_{7/2}$ and $^6P_{7/2}$ states.¹⁰ Since the ground-state multiplet contains an admixture of the $L \neq 0$ states, it can be split by the crystal field. Crystal-field splitting of the order of 0.8 K was observed for Gd^{3+} ions in yttrium-gallium garnet.¹¹ The amplitude of such a splitting is comparable to the exchange coupling and the dipolar energy in the prototype $\text{Gd}_3\text{Ga}_5\text{O}_{12}$. Thus, an accurate study of the single-ion anisotropy in the Gd-based pyrochlores is necessary to understand the magnetic properties of these materials.

To study properties of isolated Gd^{3+} ions we have pre-

pared single-crystals of non-magnetic $\text{Y}_2\text{Ti}_2\text{O}_7$ diluted with a small amount (nominally 0.5%) of Gd. The crystals were grown by traveling solvent floating zone technique. After growth the oriented single-crystals were annealed in an oxygen atmosphere. The absence of parasitic phases has been verified by powder X-ray diffraction. The magnetization of the reference sample of nominally pure $\text{Y}_2\text{Ti}_2\text{O}_7$ corresponds to no more than 0.06% of $S = 1/2$ impurities per yttrium. The lattice parameters and geometry of the oxygen surrounding of the rare-earth site are very close for $\text{Y}_2\text{Ti}_2\text{O}_7$ and $\text{Gd}_2\text{Ti}_2\text{O}_7$.¹² Hence, single-ion parameters for Gd^{3+} ions in $(\text{Y}_{0.995}\text{Gd}_{0.005})_2\text{Ti}_2\text{O}_7$ and $\text{Gd}_2\text{Ti}_2\text{O}_7$ are also expected to be very close. An electric field gradient at the Gd site in $\text{Gd}_2\text{Sn}_2\text{O}_7$ determined from the quadrupolar Mössbauer spectra⁵ is 30% smaller than that of $\text{Gd}_2\text{Ti}_2\text{O}_7$, which should lead to the corresponding decrease of the single-ion anisotropy.

Electron paramagnetic resonance (EPR) is a conventional tool to probe small crystal-field splitting of the energy levels of magnetic ions.¹³ The zero-field splitting of the multiplet leads to an easily detected change of the resonant absorption frequencies. We have used a set of home-made spectrometers with transmission type cavities for the high-frequency (20–115 GHz) measurements, and a commercial Bruker EPR spectrometer for the high-precision X-band (9.36 GHz) and Q-band (34.0 GHz) measurements.

The local surrounding of the rare-earth site in the pyrochlore structure corresponds to a trigonal point symmetry $D_{3d}(\bar{3}m)$. A general form of the single-site Hamiltonian is, then,

$$\hat{H} = B_2^0 \hat{O}_2^0 + B_4^0 \hat{O}_4^0 + B_4^3 \hat{O}_4^3 + B_6^0 \hat{O}_6^0 + B_6^3 \hat{O}_6^3 + B_6^6 \hat{O}_6^6 - g\mu_B \mathbf{H} \cdot \hat{\mathbf{S}}, \quad (1)$$

where the Stevens operators^{13,14} \hat{O}_j^i are functions of the components of the total angular momentum $S = 7/2$, with $\hat{\mathbf{z}} \parallel \langle 111 \rangle$ and $\hat{\mathbf{x}} \parallel \langle 11\bar{2} \rangle$. The lowest-order

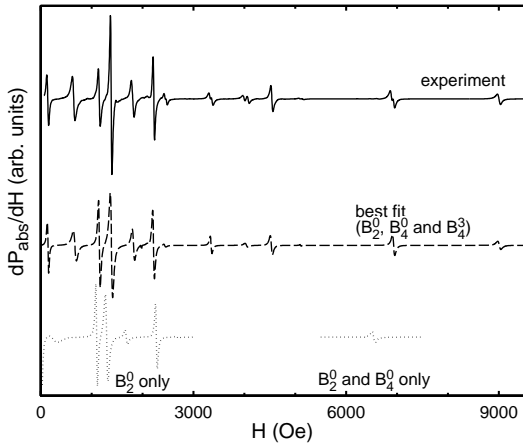


FIG. 1: Observed derivative of the 9.36 GHz microwave absorption (solid); modeled curve best fitting to the experimental results (dashed); parts of the modeled curves (dotted) corresponding to the spin-Hamiltonian constricted to the second-order term only (left) and second- and fourth-order diagonal terms (right). $f=9.36$ GHz, $\mathbf{H}||[110]$, $T=6.0$ K.

anisotropy term $B_2^0 \hat{O}_2^0$ can be rewritten up to an additive constant as DS_z^2 with $D = 3B_2^0$.

In the absence of the single-ion anisotropy Hamiltonian (1) contains only the Zeeman term. In this case the frequencies of all allowed transitions are equal and only a single resonance absorption line should be observed at a field determined by $\hbar\omega = g\mu_B H$. The measured EPR absorption spectra, see Figs. 1 and 2, contain multiple components demonstrating the presence of a non-negligible anisotropy. The analysis of the EPR spectra is complicated by the existence of four inequivalent magnetic ion positions. At high frequencies and $\mathbf{H} \parallel [111]$ it is possible to separate seven absorption components, which correspond to the spins with anisotropy axis parallel to the magnetic field direction. They include absorption component with the largest value of the resonance field and are almost equidistant (see Fig. 2). This indicates that the second order axial term (DS_z^2) is the most important one, its magnitude estimated from the total splitting of the spectra is $|D| \sim 0.25$ K. In order to refine the values of the anisotropy constants, we have modeled numerically the EPR absorption¹³ for different directions of magnetic field and different microwave frequencies trying to obtain best correspondence of the observed and modeled resonance fields values (see, e.g., Fig. 1). To determine the sign of the main anisotropy constant (resonance-field position determine only relative signs of the anisotropy constants), we have studied the temperature dependence of the intensity of different components at high microwave frequency. This analysis yielded that the main anisotropy term is of the easy-plane type and the spin Hamiltonian parameters are $g = 1.987$, $B_2^0 = (74.3 \pm 0.3)10^{-3}$ K, $B_4^0 = (5.7 \pm 0.9)10^{-5}$ K, $B_4^3 = (1.8 \pm 0.2)10^{-3}$ K. The determination of the 6-th order anisotropy parameters has been impossible due to a presence of small (0.5° or less)

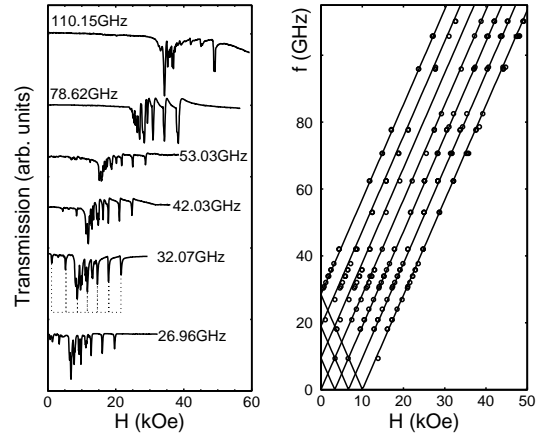


FIG. 2: Left panel: Field dependence of the microwave absorption for the high-frequency EPR spectra at $T=4.2$ K and $\mathbf{H}||[111]$. Dotted lines ($f = 32.07$ GHz) mark positions of the absorption determined by the spins with the anisotropy axis parallel to the field direction. Right panel: Field dependence of the selected resonance frequencies for the spins with the anisotropy axis parallel to the field direction ($[111]$). Solid lines give theoretical fit.

misorientation of the sample. We were able to estimate only the upper bounds: $|B_6^0| < 10^{-6}$ K, $|B_6^3| < 2 \cdot 10^{-5}$ K, $|B_6^6| < 10^{-6}$ K.

The measured value of the B_2^0 coefficient indicates that the single-ion anisotropy is the second largest interaction in the effective spin Hamiltonian of $\text{Gd}_2\text{Ti}_2\text{O}_7$. Indeed, the nearest-neighbor exchange integral is estimated from the Curie-Weiss temperature^{3,4} $\theta_{CW} = -9.5$ K as $JS^2 \approx 3.7$ K, whereas $DS^2 \approx 2.73$ K. The dipolar constant $E_{dd} = (g\mu_B S)^2 / (a\sqrt{2}/4)^3$ for the interaction between adjacent magnetic ions for above values of the g -factor and lattice parameter amounts to only $E_{dd} \approx 0.65$ K. In the following, we discuss several properties of magnetic pyrochlore materials, which might be affected by a strong single-ion anisotropy of the easy-plane type.

The first question to be addressed theoretically is whether a significant single-ion anisotropy modifies the value of the exchange constant obtained from θ_{CW} . Standard high-temperature expansion¹⁴ of the susceptibility tensor includes in general a contribution from the single-ion term $D \sum_i (\mathbf{n}_i \cdot \mathbf{S}_i)^2$:

$$\chi^{\alpha\beta} = \frac{g^2 \mu_B^2 S(S+1)}{3T} \left\{ \delta^{\alpha\beta} - \delta^{\alpha\beta} \frac{S(S+1)}{3T} \sum_j J_{ij} - \frac{2D}{5T} \left(S - \frac{1}{2} \right) \left(S + \frac{3}{2} \right) \left(\langle n^\alpha n^\beta \rangle - \frac{1}{3} \delta^{\alpha\beta} \right) \right\}. \quad (2)$$

In the case of a pyrochlore lattice the averaging in Eq. (2) has to be done over four inequivalent directions of the local anisotropy axis \mathbf{n}_i corresponding to the principal cube diagonals. Using the identity $\frac{1}{4} \sum_{i=1}^4 n_i^\alpha n_i^\beta = \frac{1}{3} \delta^{\alpha\beta}$ we find that the single-ion contribution vanishes in the second-order of the $1/T$ expansion. Therefore, the Curie-

Weiss constant is not affected by the single-ion term and is given by the same expression as in a pure Heisenberg case: $\theta_{CW} = zJS(S+1)/3$, where $z = 6$ is the number of nearest-neighbor magnetic atoms.

The unusual ordering wave-vector $(\frac{1}{2}\frac{1}{2}\frac{1}{2})$ in $\text{Gd}_2\text{Ti}_2\text{O}_7$ is probably determined by a delicate balance between the long-range dipolar interaction and several weak next-neighbor exchanges.⁸ The full analysis of the role of the single-ion anisotropy for such models lies beyond the scope of present study. We will discuss instead properties of a simplified classical spin model on a pyrochlore lattice, which takes into account only the nearest-neighbor exchange interaction and a staggered single-ion term:

$$\hat{H} = J \sum_{\langle ij \rangle} \mathbf{S}_i \cdot \mathbf{S}_j + D \sum_i (\mathbf{n}_i \cdot \mathbf{S}_i)^2 - \mathbf{H} \cdot \sum_i \mathbf{S}_i. \quad (3)$$

Transformation to classical spins of unit length $|\mathbf{S}_i| = 1$ amounts to the following redefinition of the physical parameters: $J \rightarrow JS^2$, $D \rightarrow DS^2$, $H \rightarrow g\mu_B HS$. The minimum of the Heisenberg interaction in zero field is attained for states with zero total spin on every tetrahedron: $\mathbf{S}_{\text{tet}} = \sum_{i=1}^4 \mathbf{S}_i = 0$.² The key observation for the anisotropic model (3) is that the $\mathbf{S}_{\text{tet}} = 0$ constraint is compatible with local spins being oriented perpendicular to their local hard axes: the exchange and the anisotropy terms can be simultaneously minimized.^{15,16} In particular, for one tetrahedron there is one free continuous parameter (angle), which describes the possible ground states. The remaining degeneracy of the lattice model is infinite but not extensive: the number of continuous parameters describing the classical ground state scales as $O(L^2)$ with the linear system size L . Monte Carlo investigations^{15,16} of the model (3) with $D/J = 5$ and ∞ have found a first order transition into a noncoplanar ‘ $q = 0$ ’ state at $T_c \simeq 0.13J$, which is driven by the thermal order by disorder mechanism.

To complement the above zero-field consideration we now discuss the magnetization process of the model (3). The total spin operator does not commute with the Hamiltonian in the presence of anisotropic interactions. Consequently, the magnetization plateaus, *e.g.*, the $1/2$ -plateau, do not appear on the magnetization curves of the gadolinium pyrochlores and $M(H)$ approaches the saturation value at high fields only asymptotically. Besides, the staggered (within one unit cell) single ion anisotropy might also smear phase transitions in finite magnetic fields for ‘nonsymmetric’ field orientations.

Returning back to the Hamiltonian (3) the minimum of the Heisenberg and the Zeeman interactions is given by the states obeying $\mathbf{S}_{\text{tet}} = \mathbf{H}/2J$.¹⁷ Simple extension of the zero-field consideration suggests that in weak magnetic fields spins remain in their respective local easy-planes. It is again possible to simultaneously minimize the local single-ion anisotropy terms and to satisfy the magnetization constraint. The magnetization curve is initially a straight line: $M(H) = H/8J$. The remaining degeneracy corresponds to one continuous degree of freedom per tetrahedron and $O(L^2)$ variables for the lattice

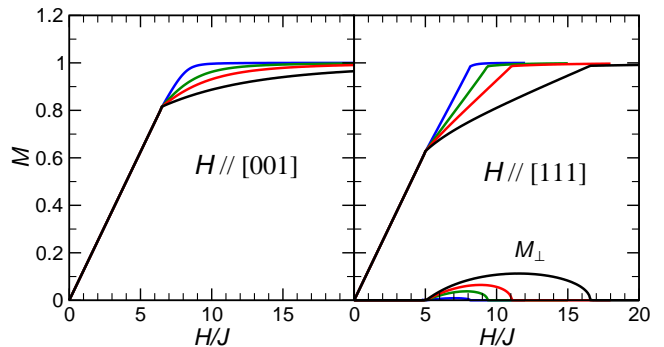


FIG. 3: (Color online) Magnetization per spin for the classical easy-plane pyrochlore antiferromagnet at $T = 0$ for the field applied along the two symmetry directions. Magnetization curves from top to bottom are drawn for $D/J = 0.2, 1, 2$, and 5. The transverse magnetization on the right panel corresponds to the same choice of D/J in the reverse order.

problem.

The situation, however, changes with increasing magnetic field. At a certain critical field H_c , which is smaller than the saturation field of the Heisenberg model $H_{\text{sat}} = 8JS$, the constraint $\mathbf{S}_{\text{tet}} = \mathbf{H}/2J$ cannot be satisfied anymore by spins lying in their local easy-planes. The degeneracy is lost and spins start to tilt out of the easy-planes towards the field direction. The corresponding critical field does not depend on the value of the anisotropy constant and is determined purely by geometry. It can be calculated analytically for fields applied along the symmetry directions of a pyrochlore lattice:

$$\begin{aligned} H_c^{[001]} &= 8J\sqrt{2/3}, & H_c^{[111]} &= 8J(3 + \sqrt{2})/7, \\ H_c^{[112]} &= 6J, & H_c^{[110]} &= 4J(1 + 1/\sqrt{3}). \end{aligned} \quad (4)$$

The fields $H_c^{[001]}$ and $H_c^{[111]}$ give, respectively, the maximal and the minimal value for $H_c(\theta, \varphi)$. The magnetization process at $T = 0$ for the above two orientations found by standard numerical minimization of the classical energy of a single spin tetrahedron is presented in Fig. 3. For $\mathbf{H} \parallel [001]$ the magnetization curve exhibits a kink at H_c and, then, the behavior of $M(H)$ becomes non-linear with full saturation $M = 1$ reached only asymptotically. A nondegenerate spin structure above H_c preserves the C_2 rotational symmetry about the field direction, which is broken at $H < H_c$. Thus, H_c describes a robust phase transition for this field orientation. The zero-temperature magnetization curve for arbitrary field orientation resembles the behavior for $\mathbf{H} \parallel [001]$. The main difference is an absence of a spin-rotational symmetry about the field direction, which may lead to a smearing of the phase transition at $H = H_c$. The other two field orientations, which have stable phase transitions at $H = H_c$ are those for the field along the $[110]$ and the $[111]$ axes. In the latter case the magnetization curve exhibits two kinks: at $H_{c1} \equiv H_c \approx 5.045J$ (4) and at a second critical field $H_{c2} > H_{\text{sat}}$, see the right panel in Fig. 3. Above H_{c2} the spin structure preserves the C_{3v} symme-

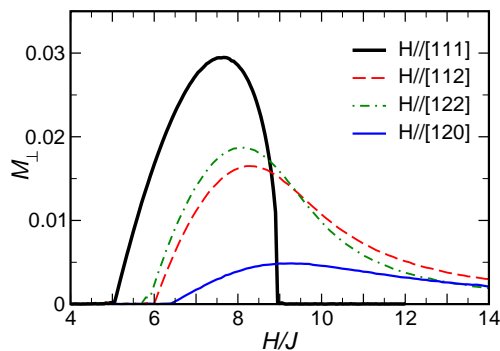


FIG. 4: (Color online) Transverse magnetization per one spin of the classical easy-plane pyrochlore antiferromagnet at $T = 0$ for $D = 0.75J$ and various field orientations.

try of the system in magnetic field, while for $H < H_{c2}$ only a mirror symmetry remains with respect to one of the three mirror planes passing through the [111] axis. Such a remaining symmetry is further lost in the low-field phase at $H < H_{c1}$. The upper transition field has an almost linear dependence on the anisotropy constant in a wide range of values for $D \lesssim 10$: $H_{c2} \approx 8J + 1.7D$. We, therefore, conclude, that for $\mathbf{H} \parallel [111]$ there are two phase transitions in magnetic field, which are smeared when the field is tilted away from this symmetry direction.

In the intermediate phase $H_{c1} < H < H_{c2}$ with broken three-fold rotational symmetry ($\mathbf{H} \parallel [111]$) the anisotropic pyrochlore antiferromagnet develops a transverse magnetization, which is shown in Fig. 3. The amplitude of the transverse magnetization grows quickly with increasing anisotropy constant D . There are, of course, three domains of \mathbf{M}_\perp oriented under 120° to each other in accordance with a broken symmetry of intermediate phase. Once magnetic field is applied away from the [111]

axis, \mathbf{M}_\perp attains a unique direction. To make connection with $\text{Gd}_2\text{Ti}_2\text{O}_7$, which according to our measurements has $D \approx 0.75J$, we plot in Fig. 4 the amplitudes of the transverse magnetization for the above ratio of D/J and for several characteristic orientations of the applied field. Though M_\perp does not exceed 3% of the saturated magnetization, the corresponding values can be definitely measured in an experiment. Such measurements would also serve as a precise method to determine the two phase transitions for $\mathbf{H} \parallel [111]$. The transverse magnetization has been previously measured in CsMnBr_3 , a triangular lattice antiferromagnet with a strong single-ion anisotropy.¹⁸ Note, that for $\mathbf{H} \parallel [001]$ and $[110]$ the transverse magnetization does not appear in the whole range of magnetic fields.

In conclusion, the measured local anisotropy of Gd^{3+} ions strongly affects magnetic properties of Gd-based pyrochlores. Though, the toy model (3) is apparently not sufficient to explain the ordered structure seen by neutrons,⁹ the quite anisotropic phase diagram in magnetic field⁶ is compatible with our experimental and theoretical findings. In particular, we have demonstrated that depending on an applied field orientation in a *cubic* crystal there are possible either one or two transitions in magnetic field. The Mössbauer measurements⁵ also agree with our ESR results pointing at ordered moments oriented perpendicular to local trigonal axes. The presented theory of the magnetization process is relevant for $\text{Er}_2\text{Ti}_2\text{O}_7$, which is a $D/J \rightarrow \infty$ realization of the model (3).

The authors acknowledge support of the Russian Foundation for Basic Research 04-02-17942, of the German Bundesministerium für Bildung und Forschung under the contract VDI/EKM 13N6917, and of the Deutsche Forschungsgemeinschaft within SFB 484 (Augsburg).

¹ *Proceedings of the Highly Frustrated Magnetism 2003 Conference*, J. Phys.: Condens. Matter **16**, S553–S922 (2004).

² J. N. Reimers, A. J. Berlinsky, and A.-C. Shi, Phys. Rev. B **43**, 865 (1991); R. Moessner and J. T. Chalker, Phys. Rev. B **58**, 12049 (1998).

³ N. P. Raju, M. Dion, M. J. P. Gingras, T. E. Mason, and J. E. Greedan, Phys. Rev. B **59**, 14489 (1999).

⁴ A. P. Ramirez, B. S. Shastry, A. Hayashi, J. J. Krajewski, D. A. Huse, and R. J. Cava, Phys. Rev. Lett. **89**, 067202 (2002).

⁵ P. Bonville, J. A. Hodges, M. Ocio, J. P. Sanchez, P. Vulliet, S. Sosin, and D. Braithwaite, J. Phys.: Condens. Matter **15**, 7777 (2003).

⁶ O. A. Petrenko, M. R. Lees, G. Balakrishnan, and D. McK. Paul, Phys. Rev. B **70**, 012402 (2004).

⁷ S. E. Palmer and J. T. Chalker, Phys. Rev. B **62**, 488 (2000).

⁸ O. Cépas and B. S. Shastry, Phys. Rev. B **69**, 184402 (2004).

⁹ J. R. Stewart, G. Ehlers, A. S. Wills, S. T. Bramwell, and J. S. Gardner, J. Phys.: Condens. Matter **16**, L321 (2004).

¹⁰ E. Antic-Fidancev, M. Lemaitre-Blaise, and P. Caro, J. Chem.Phys. **76**, 2906 (1982)

¹¹ L. Rimai and G. A. deMars, J. Appl. Phys. Suppl. **33**, 1254 (1962).

¹² B. J. Kennedy, B. A. Hunter, and C. J. Howard, J. Sol. Stat. Chem. **130**, 58 (1997); Y. Tabira, R. L. Withers, L. Minervini, and R. W. Grimes, J. Sol. Stat. Chem. **153**, 16 (2000); K. B. Helean, S. V. Ushakov, C. E. Brown, A. Navrotsky, J. Lian, R. C. Erwing, J. M. Farmer, and L. A. Boatner, J. Sol. Stat. Chem. **177**, 1858 (2004).

¹³ A. Abragam and B. Bleaney, *Electron Paramagnetic Resonance of Transition Ions*, (Clarendon Press, Oxford, 1970).

¹⁴ J. Jensen and A. R. Mackintosh, *Rare Earth Magnetism: Structure and Excitations*, (Clarendon Press, Oxford, 1991).

¹⁵ S. T. Bramwell, M. J. P. Gingras, J. N. Reimers, J. Appl. Phys. **75**, 5523, (1994).

- ¹⁶ J. D. M. Champion, and P. C. W. Holdsworth, *J. Phys.: Condens. Matter* **16**, S665 (2004).
- ¹⁷ M. E. Zhitomirsky, A. Honecker, and O. A. Petrenko, *Phys. Rev. Lett.* **85**, 3269 (2000).
- ¹⁸ S. I. Abarzhi, A. N. Bazhan, L. A. Prozorova, and I. A. Zaliznyak, *J. Phys.: Condens. Matter* **4**, 3307 (1992).